TIME DOMAIN ELECTROMAGNETIC RESISTIVITY MEASUREMENTS AT NGATAMARIKI GEOTHERMAL FIELD, NEW ZEALAND

G.F. RISK[1], T.G. CALDWELL[1&2], H.M. BIBBY[1] AND S.L. BENNIE[3]

[1]Institute of Geological and Nuclear Sciences, Wellington, N.Z.
[2]National University of Ireland, Galway, Ireland.
[3]Wairakei Research Centre, Institute of Geological and Nuclear Sciences, Wairakei, N.Z.

SUMMARY - The applicability of the time-domain electromagnetic method for determining detailed resistivity structure within a geothermal field was tested at Ngatamariki. The transient electric field vectors, which result from injection of low-frequency square-wave signals into the ground through three remote current sources, could be determined reliably for times between 0.02 and 3.3 s after each step in signal. After making small corrections for static shift, apparent resistivity pseudosections along the two measurement lines show smooth variations of resistivity from site to site. Over most of the field the images consistently show a three-layer resistivity structure with a conductive middle layer (3 – 10 Ωm) representing the conductive upper part of the thermal reservoir. A deep-seated region of low resistivity in the north-west of the field may indicate a conductive structure at about 1 km associated with a deeper diorite intrusion. Measurements sited closer than about 100 m to drillholes appear to have been disturbed by metallic casing in the holes. A change in resistivity structure in the east of the field may indicate a major geological or hydrothermal boundary.

1. INTRODUCTION

Resistivity surveying of the Taupo Volcanic Zone (TVZ), New Zealand has proved useful for delineating geothermal fields by exploiting the large contrast between the resistivity of rocks in the geothermal reservoirs and those in cold surrounding regions. However resistivity methods have been less successful for determining details of the geological structure within the fields. The experiments described here address the problem by applying the Time Domain Electro-Magnetic (TDEM) method (sometimes referred to as LOTEM). With TDEM a remote transmitter injects low-frequency square-wave signals into the ground, causing transient electric fields that are measured at the receiver. The research also adopted the practice used in seismic reflection surveying of making close-spaced measurements along lines across the field. The intention was to obtain images that are coherent from site to site and can be better correlated to the underlying hydrothermal structures than has been achieved with the traditional geoelectric methods.

An earlier experiment with the TDEM technique made at Wairakei geothermal field (Caldwell et al., 1999) was able to delineate the northern boundary of the field and deduce some details of its internal structure. This paper discusses further experiments made in March 2000 with the TDEM method in the Ngatamariki field (Fig. 1).

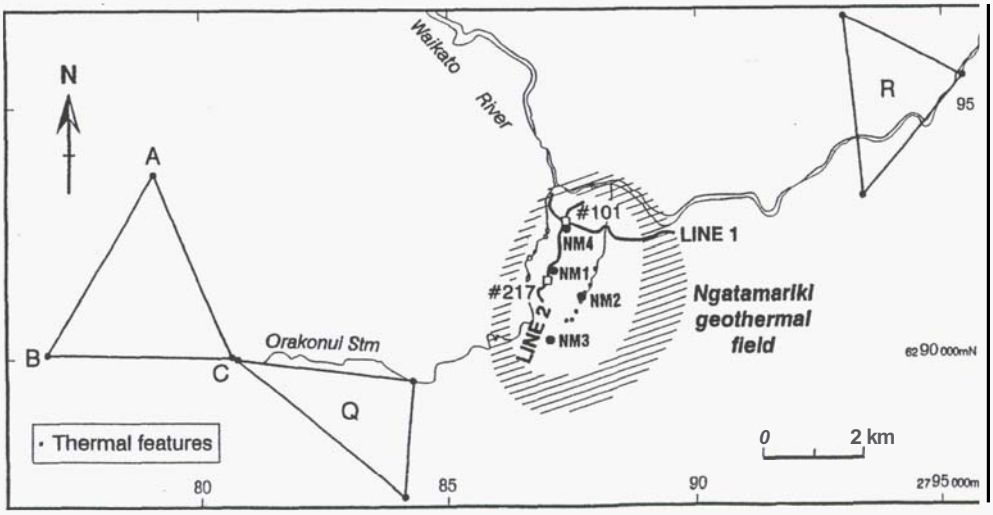

Fig. 1. Environs of Ngatamariki geothermal field. TDEM measurements were made along the bold lines within the field using signals from current transmitters A-B, B-C and C-A. Triangles Q and R show transmitters used for previous DC surveys. Transmitter T (not shown) lies about 10 km SSE of Ngatamariki. Round dots show drillholes. Shading shows inferred resistivity boundary of the field.

2. NGATAMARIKI GEOTHERMAL FIELD

A government sponsored investigation of the energy potential of the Ngatamariki geothermal field, made in the 1980s, included geophysical, geological and geochemical surveys. Four exploratory drillholes, up to 2.7 km deep, all found temperatures above 220°C. Details have been published by Bennie (1983), Browne et al. (1992), Soengkono (1992), Brotheridge et al. (1995), Christenson et al. (1997) and Arehart et al. (2002). A significant feature is the dioritic pluton encountered at 2.6 km depth in hole NM4 and its overlying zone of phyllic alteration, the only such intrusive volcanic structure known in the TVZ (Browne et al., 1992). Natural heat output from Ngatamariki is estimated at 38 – 50 MW (Bennie, 1983; Bibby et al., 1995). .Fig. 1 shows the locations of hot springs and thermally-active ground and the approximate extent of the Ngatamariki field as inferred from the resistivity surveying.

3. DC RESISTIVITY SURVEYING

Fig. 2a (after Bennie, 1983) shows the results of the resistivity profiling in the vicinity of the Ngatamariki geothermal, field made using a Schlumberger electrode array of spacing AB/2 = 500 m. The survey found very low resistivities (2 – 10 Ωm) over an area of about 5 km^2 encompassing the hot springs.

3.1. DC Multiple-Source Bipole-Dipole Method

In the multiple-source bipole-dipole method for measuring DC resistivity, three transmitting bipoles, remote from the region being surveyed, are used sequentially to inject low-frequency square-waves of current into the ground. At each field site, the three electric field strength vectors (E) are measured, and corresponding uniform-earth current densities (J_{DC}) calculated. The method of analysis by Bibby (1986) is used to fit these vectors to Ohm's Law ($E=\rho_a J_{DC}$) and define an apparent resistivity tensor (ρ_a). Tensor ρ_a is represented here as an apparent resistivity ellipse or a scalar apparent resistivity invariant (Bibby and Hohmann, 1993).

Three bipole-dipole resistivity surveys made in the 1980s (survey Q in 1984; R, 1986; and T, 1987) included the Ngatamariki region. Triangles in Fig. 1 show the locations of the current injection transmitters for surveys Q and R; that for survey T lies SSE of the figure. Triangle A-B-C indicates the transmitter used for the TDEM work in 2000.

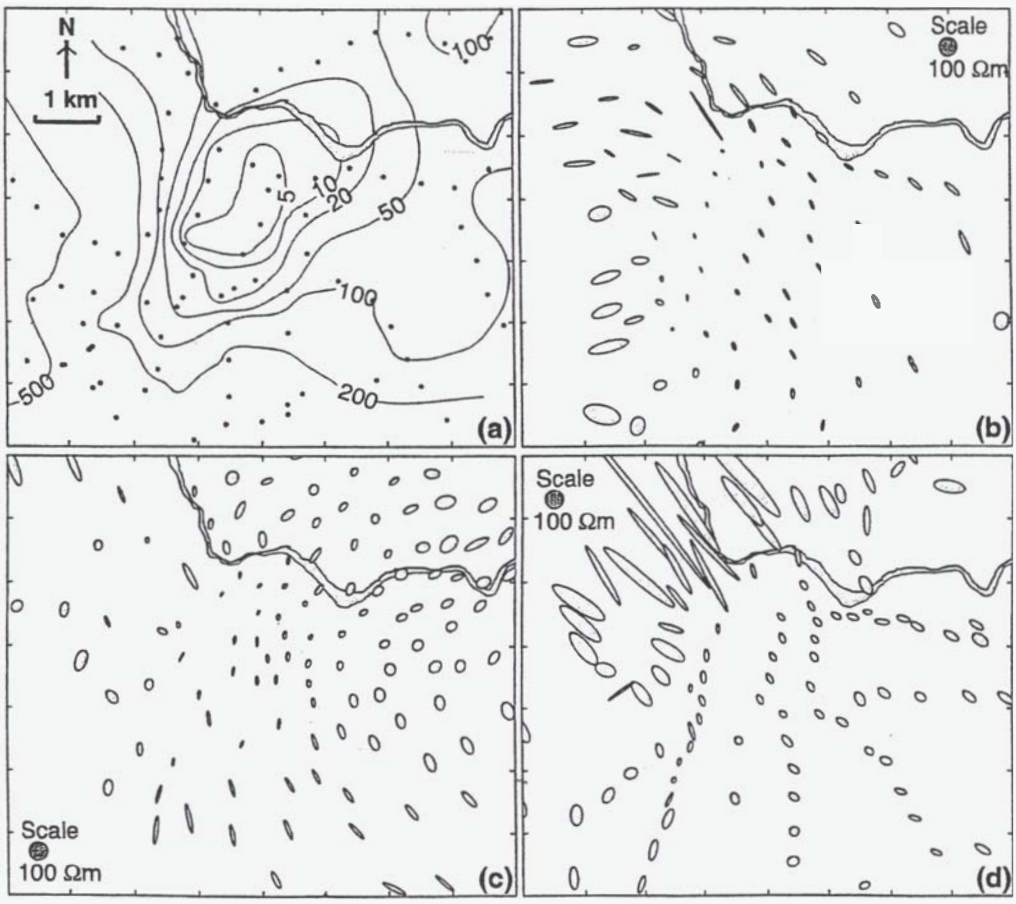

Fig. 2. Previously measured apparent resistivities at Ngatamariki.
(a) Measurements with Schlumberger array, spacing AB/2 = 500 m (after Bennie, 1983). Other diagrams show DC bipole-dipole apparent resistivity ellipses made using transmitters located in Fig. 1:
(b) transmitter Q; (c) transmitter R; (d), transmitter T.

Figs. 2b, 2c and 2d show apparent resistivity ellipses obtained from the three DC multiple-source bipole-dipole surveys. These surveys all show that resistivities within the thermal area are much lower than those measured away from the field. Very small ellipses were obtained in the region known to be thermally active. However, the sizes and patterns of the ellipses vary between surveys, reflecting the influence of regional resistivity structure and dependency on transmitter location.

4. TDEM MEASUREMENTS

The Time Domain Electromagnetic resistivity surveying method is an extension of the DC multiple-source bipole-dipole method and uses the same arrangement of three transmitters to inject currents into the ground.

4.1. Field Measurements at Ngatamariki

At each field site the two horizontal components of the electric fields were recorded using a pair of 50 m-long orthogonal dipoles attached to grounded electrodes. No magnetic fields were measured. Field measurements were made at 100 m intervals along two perpendicular measurement lines which cross the centre of the Ngatamariki field, as shown in Fig. 1.

The electric field data were recorded using a Zonge GDP-32 receiver unit which was phase-locked with the 30kW Zonge GGT30 transmitter that supplied square wave currents of centre-to-peak amplitude 20 A at frequency 0.0625 Hz. At each receiver site about 30 - 65 waveforms of data from each source bipole were recorded at 256 Hz, taking a total recording time of about 30 minutes.

4.2. Signal Processing

The first task in the processing was to identify the points at which the current steps occurred and determine the polarity of each step. Next, the time-series were divided into individual windows surrounding the signal steps. Within the windows the signal steps were aligned and their polarities rectified. Then, the 50 Hz noise was largely removed from each window by application of a digital phase-locked filter.

Finally, an iterative least-squares stacking procedure was used to fit each waveform to the sum of a step function, a cubic spline to model the transient, and a set of second-order Chebyshev polynomials to allow for long-period drifts that differed between windows. The iterative process also identified any data points that were more than three standard deviations away from the median for the previous iteration. These points were taken to be impulsive noise spikes and eliminated in calculations for the final iteration.

After rejecting data affected by the rise-time of the anti-aliasing filter in the receiver, final voltages were calculated at logarithmically-spaced intervals from 20 ms to 3.3 s after the step. The dots on Fig. 3a show the final stacked transient signals for transmitter AB (field site #217). Standard errors are of order 0.2 – 1.0 μV, smaller than the size of the dots. Fig. 3b shows the sounding curves.

4.3. Instantaneous Apparent Resistivity Tensors

For each point in the time series, an *instantaneous* apparent *resistivity tensor* $\rho_a(t)$ was derived from Ohm's law (Caldwell and Bibby, 1998).

$$E(t)=\rho_a(t)\,J_{DC}. \qquad (1)$$

Here, $E(t)$ represents the three electric field measurements and J_{DC} the corresponding steady-state (DC) uniform-half-space current density vectors. As for the DC case, each $\rho_a(t)$ is represented as an ellipse and as a scalar $P_2(t)$ apparent resistivity invariant.

5. RESISTIVITY PSEUDOSECTIONS

The P_2 apparent resistivities for the two measurement lines are plotted as pseudosections in Figs. 4a and 5a. The P_2 values form a reasonably regular pattern but at some sites systematic irregularities are evident.

Small-scale near-surface irregularities are well recognised in electromagnetic survey data as the cause of a phenomenon known as static shift. The same principles apply to TDEM data. Since static shift disturbs all resistivities on a sounding curve by a constant factor (independent of time), it can be distinguished from other disturbances for which the factor varies with time.

Static shift effects are apparent in Figs. 4a and 5a for sites at the eastern half of Line 1 and the southern end of Line 2. On the pseudosections static shifts appear as narrow vertical bands of

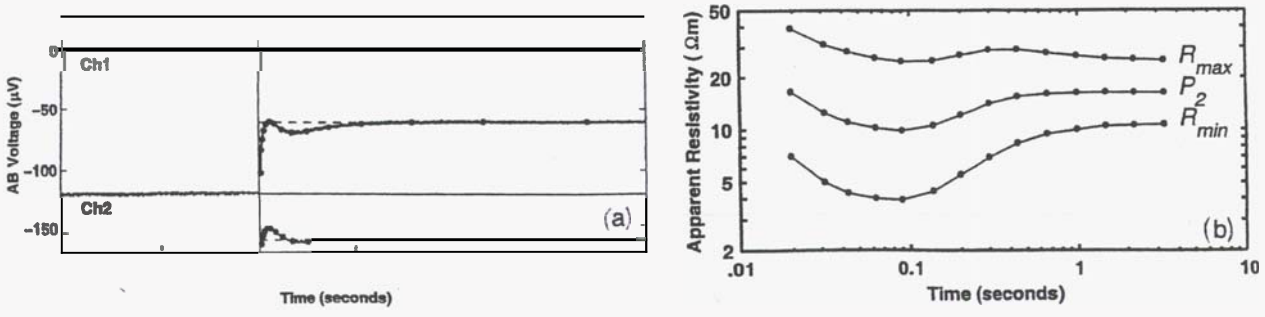

Fig. 3. Measurements from site #217. (a) Transient voltages from transmitter A-B. (b) Sounding curves.

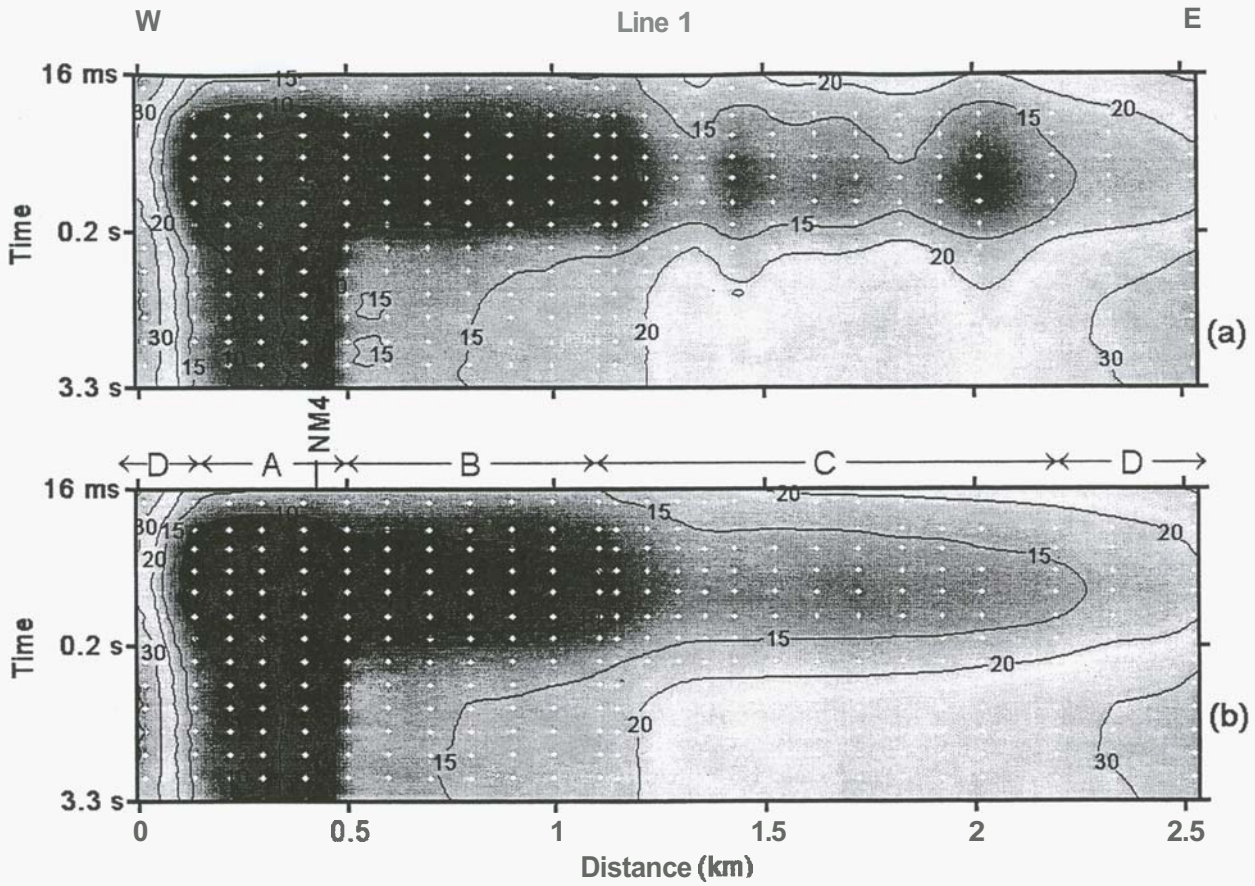

Fig. 4. Resistivity pseudo-section along Line 1 showing P_2 apparent resistivity vs. time.
(a) uncorrected; (b) corrected for short wavelength static shift.

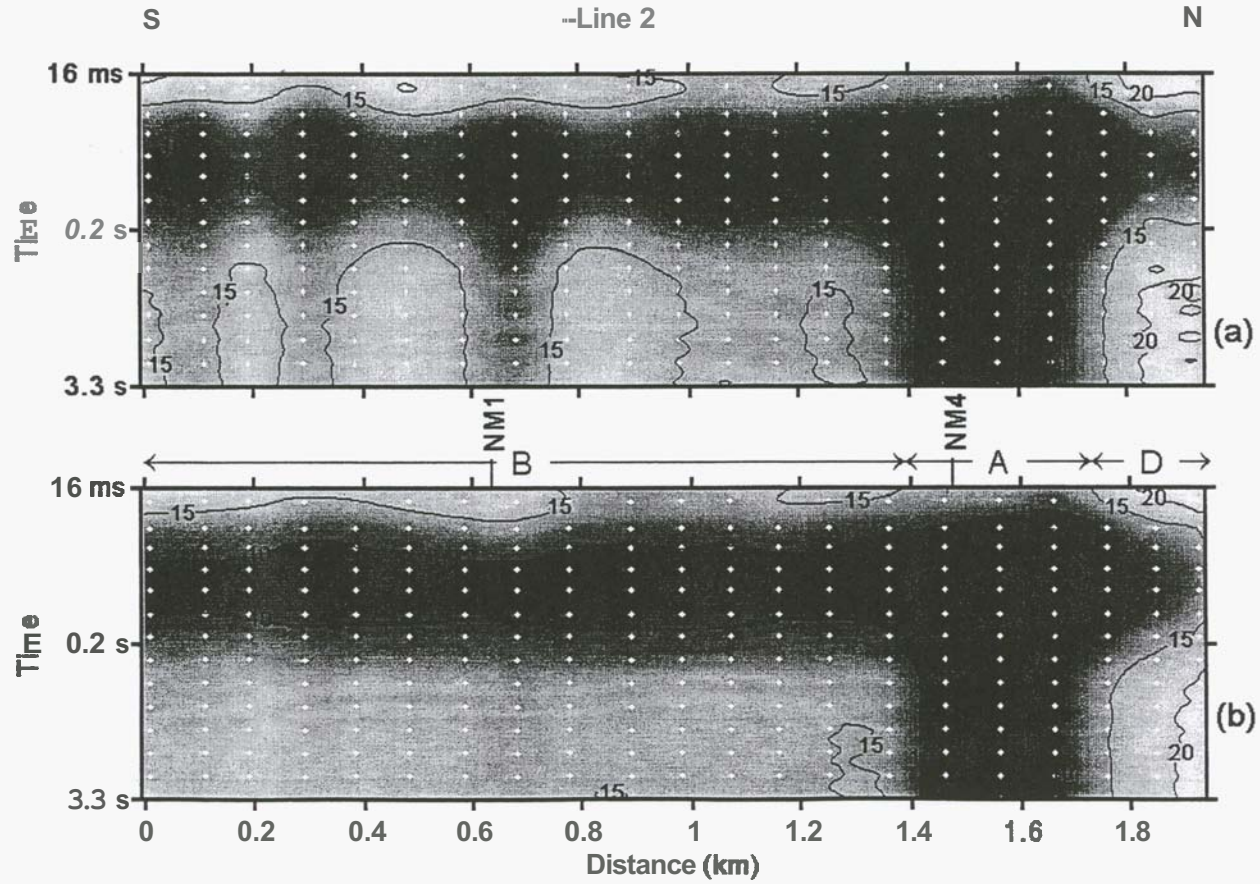

Fig. 5. Resistivity pseudo-section along Line 2 showing P_2 apparent resistivity vs. time.
(a) uncorrected; (b) corrected for short wavelength static shift.

anomalously high or low apparent resistivity and are caused by shallow-seated anomalous zones. We identified sites affected by static shift irregularities and made the appropriate corrections. The correction factors averaged 0.99 with standard deviation of 0.1; the smallest was 0.81 and the largest 1.23.

Different behavior is exhibited at sites adjacent to site #101 (Zone A) where the sounding curves are not parallel to each other. Since these data do not appear to have suffered from static shift no corrections were made.

Revised P_2 pseudosections that include static shift corrections where appropriate are shown in Figs. 4b and 5b.

6. INTERPRETATION

In Figs. 4b and 5b several distinct zones (A, B, C and D) can be identified. Zone A encompasses site #101 and the intersection of the two lines. It contains the lowest measured apparent resistivities (<10 Qm). The sounding curves and ellipses have slightly different shapes from those in other zones. In Zone B which includes the southern part of Line 2 and about 0.5 km of Line 1 east of Zone A, sounding curves have a distinctive character with a minimum at about 0.1 s. Zone C, further east on Line 1, presents similarly shaped sounding curves, but the resistivity values are about 50 percent higher. Zone D, which includes both ends of Line 1 and the north end of Line 2, shows higher resistivities reflecting the boundary of the field and the influence of resistive rocks outside the field.

6.1. Zone A

The lowest apparent resistivities of the survey (c. 5 Qm) occur in Zone A and the sounding curves have less pronounced upturns than in Zones B and C. This cannot be caused by small-scale shallow-seated irregularities. A possible explanation is the influence of the upper part of the conductive altered phyllic zone above the dioritic pluton found in drillhole NM4. Rocks in the phyllic zone, which reaches to within ca. 1 km of the surface, are rich in conductive species such as illite-smectite clays (Browne et al., 1992) and are a likely cause of most of the low resistivity anomaly in Zone A. However the disturbing effect of metallic drillhole casing in NM4 may also contribute to the anomaly, as discussed below.

6.2. Resistivity Layers in Zones B and C

Throughout Zone B the sounding curves indicate a three-layered structure which is characterised by near-surface resistivities above 20 Ωm, apparent resistivity dropping to a minimum of 5 – 10 Ωm at 0.1 s, and rising again at late time to level off at values of about 15-20 Ωm.

The relatively resistive surface layer represents non-thermal volcanics above the thermal reservoir. The prominent low-resistivity layer (<15 Qm) represents the upper part of the thermal reservoir where temperatures are high, porosities are relatively large, and the rock matrix contains an abundance of conductive minerals and clays. Resistivity increases at greater depths despite increasing temperature. This resistivity increase occurs because the abundance of the relatively conductive smectite-series clays decreases with depth due to their transformation into more resistive chlorite-dominated species.

In Zone C there is a three-layered structure similar to that in Zone B, except that all the resistivities are about 50 percent larger. A major boundary in subsurface resistivity occurs between Zones B and C (Fig. 4b) but its geological and hydrothermal nature is not known. It may represent a lateral change in geologic structure, such as a major fault or an ancient caldera structure. Since no thermal features occur east of the boundary between Zones B and C, an alternative explanation is that it may represent the eastern edge of the plume of upflowing thermal fluids at Ngatamariki or the point at which temperatures in the reservoir begin to decline horizontally.

6.3. Disturbances from Vertical Casing in Drillholes

Since the upper parts of the drillholes contain conductive steel casing there is a possibility that the casing may cause shorting or focussing effects on the imposed electric fields, thus disturbing the measurements. The measurement lines pass within 80 m of drillhole NM1 and within 40 m of NM4, and, at both sites, anomalies occurred in the measurements. A similar anomaly near a drillhole at Wairakei was noted by Caldwell et al., (1999).

While the extent of the electrical disturbance due to the buried drillhole casing is hard to assess, at least some part of the low-resistivity anomaly in Zone A appears to be caused by the casing. The anomaly near NM1 is much smaller than that at NM4 even though both are at similar distances from the respective measurement lines. This implies that the low-resistivity anomaly at NM4 is not caused by drill-casing alone; other conductors such as the conductive halo above the intrusion must contribute to the anomaly.

7. CONCLUSIONS

The experiment reported here substantiates the pioneering work of Caldwell et al. (1999) and provides a further example of the type of EM survey that will be needed for detailed imaging of resistivity structures within TVZ geothermal fields. Typical sites in this experiment were measured at a rate better than one site per hour and apparent resistivities were obtained with accuracies of 5% or less at most sites.

Several important structures have been detected. The low-resistivity layer within the Ngatamariki

field, first noted by Bennie (1983), can be clearly imaged beneath a surface-layer of higher resistivity material. Higher resistivities exist below the low-resistivity layer. The lateral resistivity boundary of the field is indicated by much higher resistivities in the north-west of the field.

Our resistivity images are unable to show much of the detailed stratigraphy evident in the drillholes. An exception is the intense phyllic alteration halo below about 1 km depth that is associated with a deeper old plutonic intrusion. Our resistivity images show a conductive structure that coincides with the alteration halo, but there remains some doubt about the extent to which the casing in drillhole NM4 contributed to the resistivity anomaly.

On Line 1, the resistivity images show a clear increase in resistivity between Zones B and C, which we infer to represent a major change in geological or hydrothermal structure. This is the type of subsurface structure that the TDEM surveying seems able to detect. However, no drillhole data are available to clarify interpretation.

Further research is planned to investigate the extent of the disturbing effects that drillhole casings have on electrical measurements in geothermal fields. Such research will be important for application of TDEM (or similar) surveying to producing fields such as Wairakei and Ohaaki which contain many drillholes. Small-scale, near-surface structures with contrasting resistivity cause static shift effects which can alter the apparent resistivities by up to 10 percent. Corrections can be readily made for static shift.

Early-time data are needed to define near surface resistivities while resistivities of deeper structures depend on the late-time data. Caldwell et al., (1999) were able to measure TDEM signals in a time window between about 0.1 to 5 s. In this work, with improved timing facilities in the receiving instruments, we were able to extend the lower end of the window to 20 ms. Further reduction of the lower limit would require revision of the way the 50Hz noise is removed. One possibility could be to make additional measurements in the frequency domain below 50 Hz, using standard analogue filters to remove the 50 Hz noise. Thus, a combination of time- and frequency-domain recording techniques may prove in practice to be most effective technique for detailed surveying of geothermal fields.

8. ACKNOWLEDGMENTS

We are grateful for skilled assistance with the field measurements from D.E Keen and D.J. Graham. The New Zealand Foundation for Science, Research and Technology supported this work through contract C05X0004. This paper is IGNS contribution No. 2405.

9. REFERENCES

Arehart, G.B., Christenson, B.W., Wood, C.P., Foland, K.A., Browne, P.R.L., 2002. Timing of volcanic, plutonic and geothermal activity at Ngatamariki New Zealand. J. Volcanol. Geotherm. Res. 116,201-214.

Bennie, S.L., 1983. Geophysical investigations of the Ngatamariki geothermal area. Geophysics Division Report No. 192, Department of Scientific and Industrial Research, Wellington, 35p.

Bibby, H.M., 1986. Analysis of multiple-source bipole-dipole resistivity surveys using the apparent resistivity tensor. Geophysics 51, 972-983.

Bibby, H.M., Caldwell, T.G., Davey, F.J., Webb, T.H., 1995. Geophysical evidence on the structure of the Taupo Volcanic Zone and its hydrothermal circulation. J. Volcanol. Geotherm. Res. 68, 29-58.

Bibby H.M., Hohmann, G.W., 1993. Three dimensional interpretation of multiple-source bipole-dipole resistivity data using the apparent resistivity tensor. Geophys. Prosp. 41 679 – 723.

Brotheridge, J.M.A., Browne, P.R.L., Hochstein, M.P., 1995. The Ngatamariki geothermal field, NZ: surface manifestations – past and present. Proc. 17th New Zealand Geothermal Workshop, University of Auckland, pp. 61-66.

Browne, P.R.L., Graham, I.J., Parker, R.L., Wood, C.P., 1992. Subsurface andesite lavas and plutonic rocks in Rotokawa and Ngatamariki geothermal systems, Taupo Volcanic Zone, New Zealand. J. Volcanol. Geotherm. Res. 51, 1999-215.

Caldwell, T.G., Bennie, S.L., Keen, D.E., Graham, D.J., 1999. Long-offset transient electromagnetic measurements at the Wairakei geothermal field. Proc. 21st New Zealand Geothermal Workshop, University of Auckland, pp. 133-138.

Caldwell T.G. and Bibby H.M., 1998. The instantaneous apparent resistivity tensor: a visualisation scheme for LOTEM electric field measurements. Geophys. J. Int. 135, 817-834.

Christenson, B.W., Mroczek, E.K., Wood, C.P., Arehart, G.B., 1997. Magma-ambient production environments: PTX constraints for paleo-fluids associated with the Ngatamariki diorite intrusion. Proc. 19th New Zealand Geothermal Workshop, University of Auckland, pp. 87-92.

Soengkono, S., 1992. Magnetic anomalies over the Ngatamariki field, Taupo Volcanic Zone, New Zealand. Proc. 14th New Zealand Geothermal Workshop, University of Auckland, pp. 241-246.